Materials Science & Engineering A 748 (2019) 21–29

Contents lists available at ScienceDirect

Materials Science & Engineering A

journal homepage: www.elsevier.com/locate/msea

Development of a novel methodology to study fatigue properties using the small punch test

R.J. Lancaster[a,*], S.P. Jeffs[a], H.W. Illsley[a], C. Argyrakis[b], R.C. Hurst[a], G.J. Baxter[b]

[a] Institute of Structural Materials, College of Engineering, Swansea University Bay Campus, Swansea SA1 8EN, United Kingdom
[b] Rolls-Royce plc., P.O. Box 31, Derby DE24 8BJ, United Kingdom

ARTICLE INFO

Keywords:
Titanium alloys
Small punch test
Fatigue
Fractography
Finite element analysis
Numerical correlations

ABSTRACT

Small scale mechanical test methods are now widely recognised as an established and quantifiable means of obtaining useful mechanical property information from limited material quantities. Much research has been gathered employing such approaches, but to date these methods have largely been restricted to characterising the creep, tensile and fracture characteristics of numerous materials and alloys through the small punch (SP) test. Clearly, a key element that is missing from this list of fundamental mechanical properties is understanding the cyclic response of the material, a significant form of damage that accounts for a large proportion of in-service failures in critical structural components. Therefore, in order to profit from the numerous benefits that SP testing has to offer, including a small sample size and hence reduced cost, a small scale fatigue testing methodology is now required to provide a holistic mechanical property evaluation. Such an innovative approach would provide real potential benefit to the engineering mechanical characterisation community. This paper will discuss the development and implementation of this highly bespoke SP fatigue testing methodology that can accommodate alternative loading ratios and frequencies to mimic conventional fatigue data. A number of novel experiments have been performed on the titanium alloy Ti-6Al-4V with accompanying analysis and fractography detailed. Numerical correlations to uniaxial fatigue data is also presented through the use of Finite Element Analysis.

1. Introduction

When considering a material to be employed for any structural component, a fundamental understanding of the material's mechanical properties is an essential requirement. However, performing an extensive mechanical assessment of any novel material still at the development stage can be an expensive activity when accounting for the relatively large volume of material required and restricted material availability. Such scenarios have previously led to the employment of small scale test procedures, in particular, the small punch (SP) test. The SP test has found application in obtaining creep, tensile and fracture data from limited quantities of material, thus offering a significant cost saving whilst providing key mechanical property information from highly localised, discrete regions. Previous examples of the technique's applicability is the determination of the creep properties of heat affected zones (HAZ) of welded joints [1–3] and to assess the level of neutron irradiated damage in nuclear pressure vessels [4–6]. More recently, the SP test has been recognised for its unique potential in assessing the mechanical performance of novel materials for aero engine applications, where substantial quantities of experimental material cannot easily be produced to allow characterisation by conventional mechanical test approaches [7]. This has arisen from the continuous evolution of the jet engine as materials scientists and engineers strive for ever increasing operating temperatures and weight savings to improve engine efficiency in line with the ACARE2020 targets [8]. As such, SP testing can offer an attractive option of determining the mechanical properties of novel alloy variants at the early stage of development for alloy down selection.

The SP test is a complex miniaturised test procedure where a miniature disc sample is subjected to an applied compressive force that is transferred through a punch indenter onto the upper surface of the disc. The loading may be applied under a constant force, promoting a creep type deformation response, or alternatively under a constant displacement rate, thus promoting a more tensile behaviour. The compressive loading occurs as the punch tip imparts a load on the disc sample, leading to the most dominant stage of deformation where the membrane around the punch tip begins to stretch. From here, the membrane deforms in a biaxial tensile manner and thinning occurs through the

* Corresponding author.
E-mail addresses: r.j.lancaster@swansea.ac.uk (R.J. Lancaster), s.p.jeffs@swansea.ac.uk (S.P. Jeffs), 634576@swansea.ac.uk (H.W. Illsley), christos.argyrakis@rolls-royce.com (C. Argyrakis), r.c.hurst@planet.nl (R.C. Hurst), gavin.baxter@rolls-royce.com (G.J. Baxter).

https://doi.org/10.1016/j.msea.2019.01.074
Received 7 January 2019; Received in revised form 18 January 2019; Accepted 19 January 2019
Available online 25 January 2019

cross-section of the material. The initial bending and biaxial loading observed in this test approach contrasts to the deformation behaviour experienced in a conventional test arrangement where the specimen simply elongates under an applied uniaxial tensile force. However, despite the differences in deformation behaviour, it has been proven that creep data sets can be correlated through the k_{SP} approach [9–11], which is detailed in the European Code of Practise (EUCoP) for small punch testing [11]. Furthermore, effort has been made in defining fundamental mechanical properties from SP tensile results, with values for ultimate tensile strength (σ_{UTS}), yield and proof stress now finding interpretation from several sources [12–15].

Despite the progress that SP testing has made in becoming an established means of assessing the creep and tensile properties of limited material volumes under various temperature and environmental conditions, there is still a clear need to understand the cyclic deformation behaviour of a volume of similar dimensions. Fatigue failure of structural components is one of the major issues that mechanical designers strive to overcome as fatigue can typically develop with no appreciable sign and fracture catastrophically with little warning. As such, an accurate estimation of life for fatigue damaged material is of significant importance and requires the utmost attention not just by the larger scale testing community, but also researchers and engineers exploring smaller scale test approaches.

To date, effort in realising a small scale fatigue test methodology has been extremely limited with the majority of research having taken place in the Indian Institute of Technology Madras [16,17], where the cyclic automated ball indentation (ABI) method was adopted. Here, Prakash et al. [17] employed the technique to characterise the mechanical performance of bulk material, but this method was found to be limited in application and not suitable for thin walled components, such as a small punch disc specimen. The same author then designed a cyclic loading arrangement to accommodate the dimensions of a SP disc with a series of experiments performed under a compressive loading ratio, or an $R > 0$ [17]. In this research, the hysteresis energy accumulated was estimated as the area beneath the loading and subsequent unloading of the force-displacement curves during the duration of the test. Results showed that the cumulative energy generated exhibited a three stage response, akin to the behaviour typically seen in a traditional SP creep test, with distinct regions of primary, secondary and tertiary deformation, with the onset of cracking and failure occurring during the transition to the final stage [17]. This approach is clearly innovative and novel, but further effort is necessary to truly understand the damage behaviour of the material and how this can be compared to traditional fatigue results. Furthermore, there is little evidence of any classical fatigue features in supporting post-test examinations of the tested discs, indicating that further research is required.

This paper will present a series of mechanical tests on the titanium alloy, Ti-6Al-4V, a material chosen based on the wealth of literature published on the fatigue behaviour of this material [18,19]. Ti-6Al-4V is widely regarded as the optimal material for jet engine fan blade applications, due to its excellent combination of properties including a high strength to weight ratio. Given the nature of fatigue damage that is particularly prominent for such components, an understanding of the cyclic behaviour is clearly important. This research will discuss the progress made in developing an innovative small punch fatigue (SPF) testing methodology capable of generating cyclic deformation information on Ti-6Al-4V that can be correlated to data gathered from traditional uniaxial fatigue approaches on the same alloy. Such a correlation will contribute significant added value to the test technique in providing validation to uniaxial approaches, giving potential users further confidence in utilising the method to characterise alternative material systems. Supporting fractography will provide evidence of the evolving fatigue damage in the miniature disc specimens and indicative features that correspond to fatigue, with effort made in correlating the results to strain controlled uniaxial fatigue (UF) data using empirical and numerical approaches.

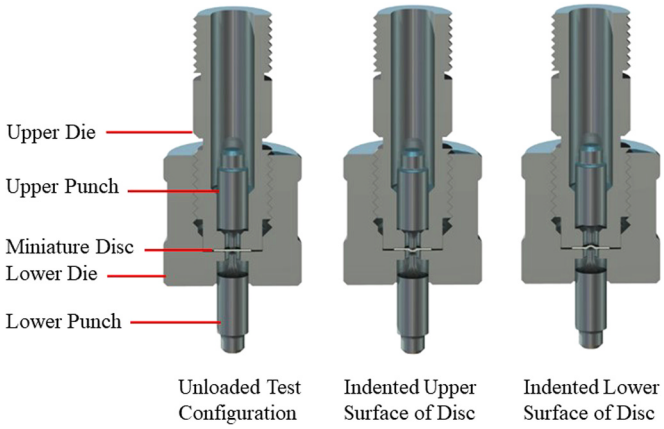

Fig. 1. Schematic representation of the small punch fatigue (SPF) experimental setup.

2. Experimental procedures

2.1. Experimental set-up

Small punch fatigue (SPF) tests were performed on a novel SP fatigue test jig developed by the authors for insertion into the load train of a servo-actuated universal test frame. The jig comprises of a ± 5 kN load cell to ensure accurate control of the applied forces with a good level of sensitivity and a twin-punch system from which both sides of the SP disc specimen can be indented, i.e. to replicate a fully reversed loading cycle or $R = -1$. The two hemispherical ended punch indenters both have a 2 mm diameter, with one positioned above the SP specimen within the upper die and the other directly beneath the specimen located within the lower pull rod, in order to impart a force on the underside of the disc. The test specimen is then vertically cycled, with each punch deforming the relevant face in turn, thus giving an $R = -1$ loading ratio. During this cycle, as the force was removed in either tension or compression, a small residual force in the order of 100 N was held on the material to ensure no air gap developed in the load train. This test configuration is displayed in Fig. 1. In either test arrangement, the deformation on each face was monitored every $5 * 10^{-3}$ s via two linear variable displacement transducers (LVDTs), in addition to the position and force measurements recorded from the test frame. Since this test procedure is envisaged to be employed for elevated temperature experiments in future research programmes, all components of the jig, including both punches, were made from Nimonic-90 to eliminate any potential issues relating to mismatching thermal expansion coefficients.

In the die set, the SP disc specimen is clamped within the upper and lower dies, both of which have receiving hole diameters of 4 mm, dimensions that comply with the directives detailed in the EUCoP [11]. As mentioned, an internal hydraulic system is employed to ensure that throughout the test the two indenters maintain contact with the disc, taking into account the thinning of the centre of the specimen cross section due to loading and to ensure no air gap develops.

2.2. Material and specimens

The study was carried out on the aerospace titanium alloy Ti-6Al-4V. The material was extracted from a disc forging and exhibits a bimodal microstructure consisting of predominantly equiaxed α and β grains with randomly orientated texture on all orthoganol planes, as displayed in Fig. 2. The material contains a primary alpha grain size of 20 μm and a volume fraction of 60% primary alpha.

The forged material was machined into cylindrical uniaxial fatigue specimens with a 6 mm diameter and tested at room temperature in strain control under an $R = -1$, 0.25 Hz trapezoidal waveform. These

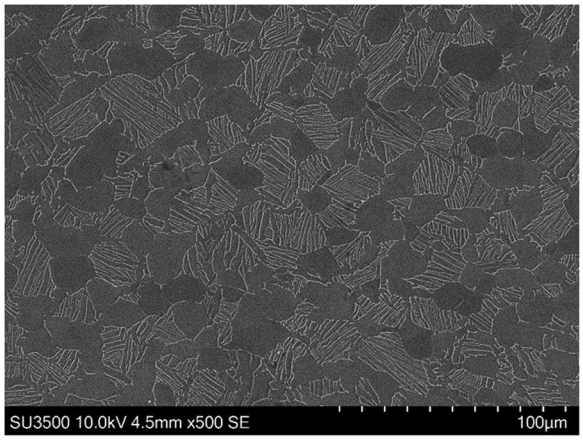

Fig. 2. Microstructure of forged Ti-6Al-4V.

results provided the data for the uniaxial to SPF comparison for fully reversed loading conditions. Upon failure, the threaded ends of the uniaxial specimens were machined down to 9.5 mm diameter cylinders. SP specimens were then prepared by sectioning slices approximately 800 µm in thickness from the cylinders and grinding them with progressively finer grit papers until a 500 µm ± 5 µm thickness was achieved with a highly polished finish. These preparation procedures are in accordance to the directives stated in the EUCoP [11]. Uniaxial fatigue data for R = 0.1 was sourced from [20].

3. Results and discussion

3.1. Small punch fatigue (SPF) results

A series of SP fatigue tests were performed at ambient room temperature on forged Ti-6Al-4V to generate representative force (F) – number of fatigue cycles to failure (N_f) curves, or F-N curves. Tests were performed under two loading ratios: R = −1 to simulate a fully reversed loading cycle and R = 0.1 to give a near zero to maximum response whilst eliminating any cycling effects through zero force. For each of the experiments, loading was applied using a sinusoidal waveform with a frequency of 1 Hz. All tests were performed at ambient room temperature.

Fig. 3(a) presents all the SPF test results in the form of F_{MAX} against N_f. Both sets of data show excellent consistency, producing R^2 values of 0.97 for R = 0.1 and 0.91 for R = −1 respectively. It is evident from the $F_{MAX} - N_f$ plots that the behaviours seen across the two R ratios are highly comparable to the response that would typically be expected from a uniaxial stress (σ) – number of fatigue cycles to failure (N_f) curve for the same material (Fig. 3(b)) where, as the F (or σ) value applied to the specimen is increased, the number of cycles required to produce failure decreases. The influence of R ratio across both SPF and UF test types is also similar, with R = 0.1 or R = 0 results having a superior response to the fully reversed data (R = −1) when compared as F_{MAX} (or σ_{MAX}). Furthermore, if the results are recalculated and compared as a F (or σ) range response, the trend is inversed and the R = −1 data shows a superior performance for both SPF and UF.

For each SPF test, a series of data was generated capturing the evolving deformation in each disc specimen. Fig. 4 shows the evolution of disc displacement for each of the SPF tests and how the upper and lower surface displacement values behave during the duration of each. Fig. 4(a) shows this behaviour for the R = 0.1 results and a clear transition can be seen between the stages of crack initiation and the onset of rapid propagation as the discs approach failure. In each test, cyclic loading was interrupted once a displacement range of 250 µm was achieved, from which a clearly defined crack was identifiable. At this point, the disc was considered fractured and the test was

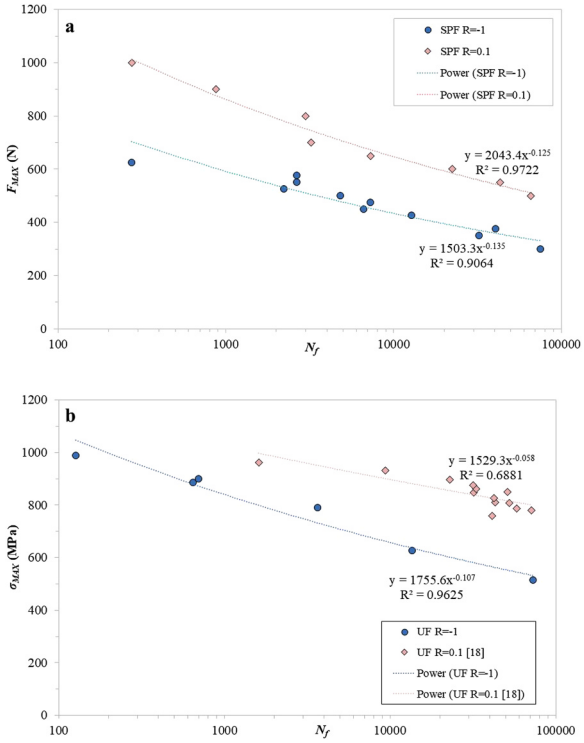

Fig. 3. Fatigue behaviour of Ti-6Al-4V at 20 °C under a) SPF and b) UF [20] loading.

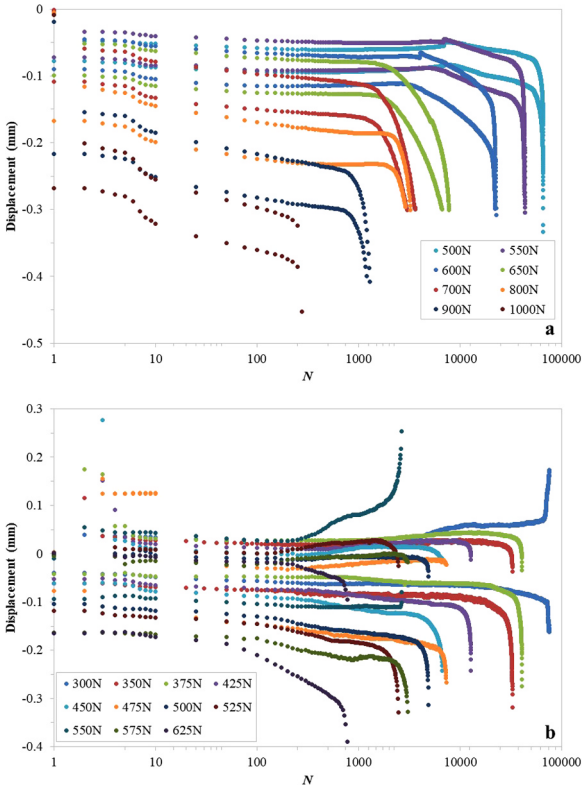

Fig. 4. Upper and lower disc displacement behaviour for SPF tests on Ti-6Al-4V specimens performed at 20 °C at a) R = 0.1 and b) R = −1.

terminated. This criterion was established from a series of experimental trials that took place prior to testing. A similar trend is observed in Fig. 4(b) which presents the displacement evolution in the R = −1 SPF experiments. Here, the results indicate that disc deformation is

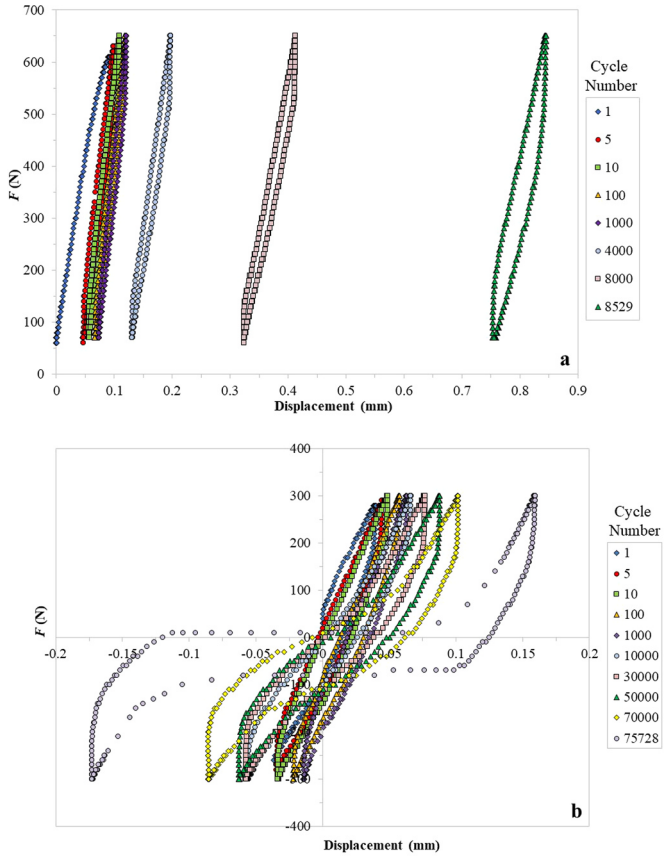

Fig. 5. Hysteresis force-displacement loops for a SPF test on a Ti-6Al-4V specimen performed at 20 °C at a) R = 0.1 (F_{MAX} = 650 N, N_f = 7300) and b) R = −1 (F_{MAX} = 300 N, N_f = 75375).

predominantly more prevalent on the lower surface of disc, or from the lower punch penetrating into the lower surface of the material. This relates directly to the nature of the loading waveform, where the applied force in the R = −1 cycle always commences in this manner, where the first part of the cycle exerts a force onto the lower surface of the disc. As such, the lower surface of the disc will tend to experience a faster rate of crack growth compared to the upper surface as the crack will usually initiate on the lower surface first.

This information, together with regular force recordings taken from the control and monitoring software, enabled the generation of hysteresis force-displacement loops. Fig. 5(a) presents the force-displacement loops for a SPF test performed under an R = 0.1 and a maximum force of 650 N.

The image helps to illustrate the consistency of the applied loading waveform throughout the whole test, where the maximum and minimum force values maintain excellent control throughout. The loops also provide quantifiable information regarding the accumulation of plastic deformation of the disc. In this test the maximum applied force was high enough to already activate the stage of membrane stretching in the first cycle [21,22] and this is reflected by the level of displacement seen. From here, the loops become more stabilised before the volume of plastic displacement increases as the disc approaches failure (loop 8529). This is seen more clearly in Fig. 5(b) which depicts the loops generated under an R = −1 loading ratio. Again, the width of the loops for the initial cycles is quite limited, but as the disc completes an increasing number of fatigue cycles and starts to approach a stabilised condition or beyond, the thickness of the loops become much wider. This behaviour replicates the progression of stress-strain loops observed in a component when subjected to more traditional fatigue testing procedures. In a SPF test however, the loops in a R = 0.1 test can be seen to drift as the centre of the miniature disc is unable to retain its original clamped position due to the extent of permanent deformation generated in the material.

3.2. Small punch fatigue (SPF) fractography

Following testing, fractographic investigations were undertaken on a selection of the SP specimens. Fig. 6 presents the fracture morphology for a test performed under an R = 0.1 and F_{MAX} = 650 N. The disc appears to be dominated by a star-like cracking morphology with the cracks growing in a radial manner from the central region of the disc. As the disc accumulates an increasing number of SPF cycles, crack growth becomes more extensive, stretching the membrane further until it is unable to withstand the applied force. This behaviour is evident across each of the SPF tested specimens under the two loading ratios. However, in the samples that were tested under an R = 0.1, additional features were present that were relative to fatigue damage. In uniaxial fatigue tests, crack growth in a material is usually accompanied by the formation of striations, markings on the crack path that provides sufficient evidence that the component has indeed experienced a form of fatigue damage. Striations are defined as features that typically represent the increment of crack growth that occurs in a single loading cycle through the plastic blunting process. These can be seen in Fig. 7 which depicts a fracture surface from a uniaxial strain-controlled fatigue test on Ti-6Al-4V under a loading ratio of R = 0. Striations can be seen emanating from the site of crack initiation at the edge of the specimen, progressing in a perpendicular direction across a large portion of the fracture surface. Similar features are also observed in the SPF test (Fig. 6), with striations developing from the central region (or the crack origin) and progressing outwards with crack growth. Near the central portion of the disc, the striations are spaced in close proximity to one another, verifying the slower rate of crack growth during the early stages of the test. The distance between the striations then increases as the crack propagates through the material, reflecting a faster rate of crack growth and a behaviour that is synonymous with fatigue damage under more recognised testing approaches. However, the evidence of striations in a SPF test is limited to R = 0.1, as the compressive nature of the fully reversed tests (R = −1) eliminates such features as the disc cycles through zero force in each fatigue cycle. As such, any striations that may have been present in the radial cracks were worn away by the crack opening-closing procedure.

3.3. Striation counting

Since only vestiges of striations were observed on the specimens which had been tested with a fully reversed loading cycle, the lack of continuous visible striations made counting striations across an entire fracture surface of these specimens unfeasible. For the tests performed with a loading ratio of R = 0.1, however, the crack is not completely closed during each cycle and striations on the fracture surface are preserved.

Striations observed on the fracture surfaces of the tests performed with a loading ratio of R = 0.1 were imaged in a systematic manner along the length of the crack through the thickness of the specimen as depicted in Fig. 8. For each image, a series of five measurements were taken of the width of 10 striations using ImageJ image processing and analysis software. From these measurements, the mean striation width was calculated. The SEM stage coordinates were also recorded at the location of each image as well as the crack initiation point, from which the length of the crack at each image location was determined. Fig. 9(a) shows the average distance between striations plotted against crack length for a SP fatigue test specimen tested at R = 0.1. The distance between striations and hence crack growth rate increases with crack length, similar to what would be expected during traditional fatigue damage.

The total number of striations to failure was estimated from the area

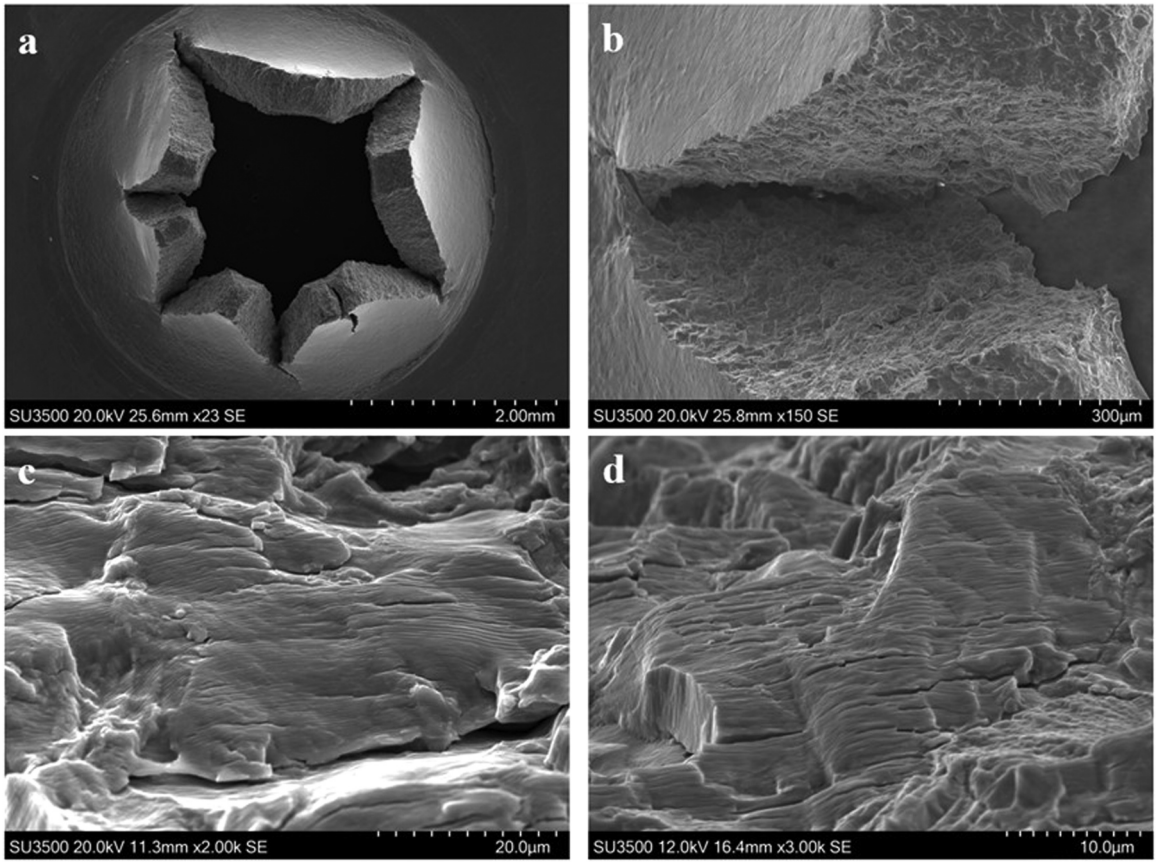

Fig. 6. SEM fractographic images of a SPF test on a Ti-6Al-4V specimen tested at 20 °C, R = 0.1, F_{MAX} = 650 N, N_f = 7300 a) overall fracture surface, b) nature of secondary crack c) evidence of striations near the start of the crack initiation point and d) evidence of striations further along the progressing crack.

under a curve for striation density against crack length, a method which has been successfully employed by Hershko et al. [23]. Fig. 9(b) presents these results, illustrating that a significantly higher striation density is observed closer to the crack initiation point, decreasing towards the end of the striated crack length. The area under the curve was found by integration between limits defined by the striated crack growth to give an estimate of the striations to failure for that specimen. For the data shown in Fig. 9(b), integration of the equation for the curve between 0 and 0.41 gives a value of 761. Whilst also accounting for scatter, comparing this value to the number of cycles to failure for this specimen of 850 shows good agreement (approximately 10.5% difference) and that the life to initiation is a small proportion of the total life.

3.4. Correlations to uniaxial fatigue data

Even though SPF and UF results appear to produce a similar *σ/F-N* response and fracture surface features, thus providing confidence in the SPF test arrangement, the manner of material deformation has contrasting behaviour. During a SP test, whether the force is applied to

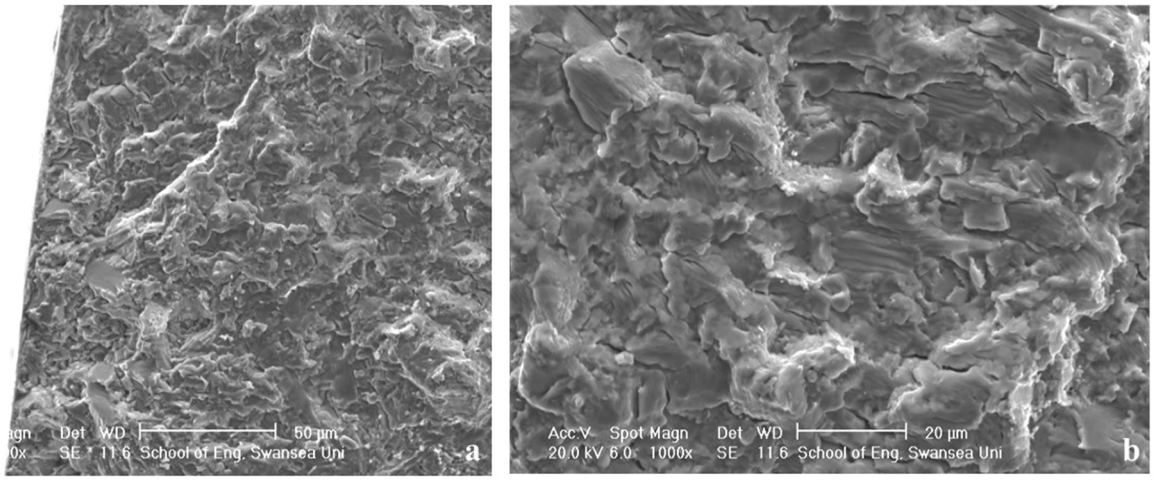

Fig. 7. SEM fractographic images of a UF test on a Ti-6Al-4V specimen tested at 20 °C, R = 0, ε_{MAX} = 1%, N_f = 8400 a) fatigue initiation zone and b) evidence of striations on the fatigue surface.

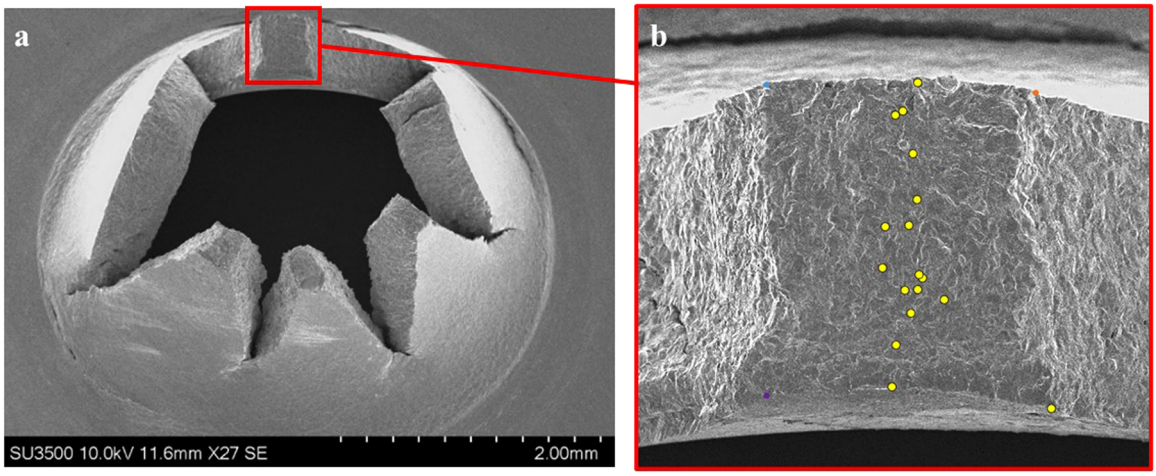

Fig. 8. Location of images used to count striations across thickness of SP fatigue fracture surface.

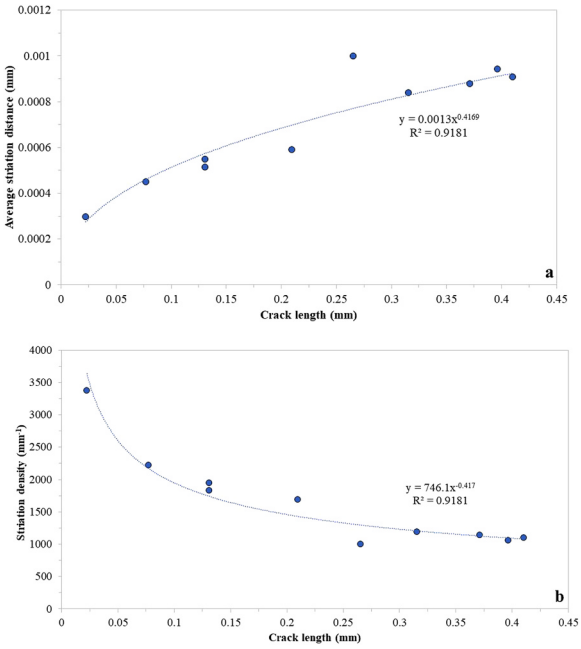

Fig. 9. a) Average striation distance against crack length, b) Striation density against crack length.

replicate a tensile, creep or fatigue mode of damage, the miniature disc is initially subjected to a small period of elastic deformation through an applied compressive force, which is quickly followed by a bending motion and tensile elongation around the periphery of the punch head. This behaviour has previously been well documented [24,25] and many sources assume Chakrabarty's theory of membrane stretching [26] to understand such phenomena. As the SP disc endures these various states of evolving damage, the disc is continuously deforming under a transient biaxial stress condition. This differs from the modes of deformation experienced in a more traditional, uniaxial testing arrangement where the specimen will typically elongate under a uniaxial tensile force, whether the force is applied in a cyclic, dynamic nature to promote fatigue or statically to stimulate tensile deformation. Therefore, the biaxial behaviour observed in a SP test must be considered when attempting to correlate SPF data to uniaxial results, particularly if the investigated material tends to have strong anisotropic properties or a heavily textured microstructure. As such, many stress engineers sometimes struggle to accurately mimic the conditions seen in a SP test and correlate such data to uniaxial test results.

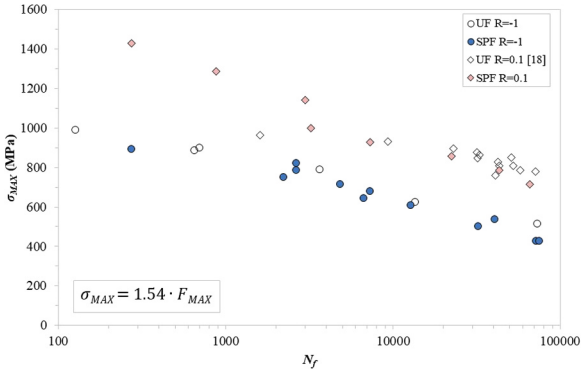

Fig. 10. Correlation between SPF and UF results.

3.4.1. Empirical approaches

Several sources [10,12,27,28] have used empirical methods to relate creep and tensile data sets from the differing test methods. Fig. 10 correlates the SPF and UF results revealing the ratio of F_{MAX}/σ_{MAX} to be 0.65 for both loading regimes, which in each case achieves optimal R^2 values, a measure of data consistency, for the combined data sets such that $R^2 = 0.91$ for $R = -1$ and 0.89 for $R = 0.1$.

This rudimentary correlation suggests that the apparent σ_{MAX} in a SPF test is $1.54 \bullet F_{MAX}$ and while it is promising that the same solution is determined for the different R values, utilising fundamental stress analysis equations that apply to the test arrangement may reveal whether this correlative ratio could be considered practical. It is important to note that the σ_{MAX} values determined for $R = -1$ are reasonable in their magnitude with the SPF and UF data that has been correlated for a similar range of cycles to failure. However, the available UF data correlating $R = 0.1$ does not include any results for $N_f < 10000$ and the apparent σ_{MAX} in the lower life SPF experiments ($N_f < 3000$) exceed the ultimate tensile strength (σ_{UTS}) of the Ti-6Al-4V material at room temperature (1046 MPa).

Through the first cycle up to F_{MAX} in the SPF test arrangement, the specimen can be considered to be a circular disc, uniformly loaded with the edges clamped. Taking the assumption that the deflection is small compared to the thickness, the maximum deflection, y_{MAX} and maximum stress σ_{MAX} can be estimated through the following equations [29]:

$$y_{MAX} = \frac{P \bullet r^2}{16\pi D} \tag{1}$$

$$\sigma_{MAX} = \frac{6P}{4\pi t}(1+\nu)\ln\left(\frac{r}{e'}\right) \tag{2}$$

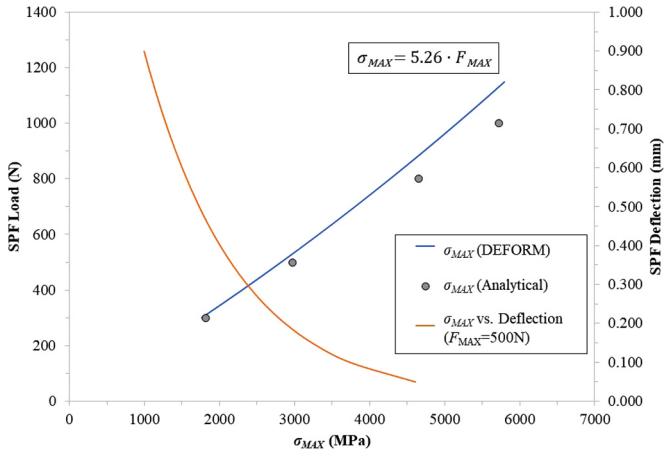

Fig. 11. Estimation of σ_{MAX} vs. SPF load during initial loading (analytical and simulated) and σ_{MAX} vs. specimen deflection for F_{MAX} = 500 N.

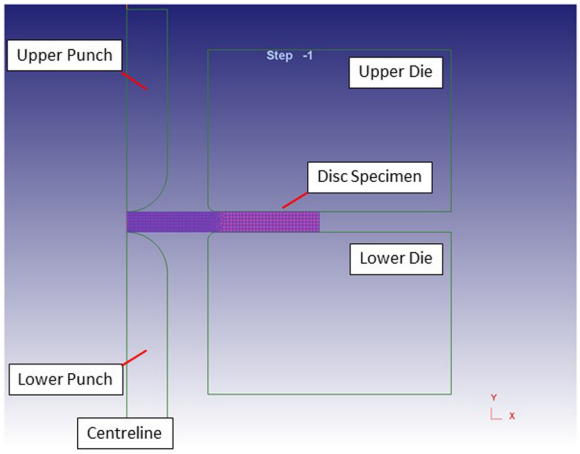

Fig. 12. Axisymmetric model of the SPF experimental setup and the mesh employed using FEA DEFORM software.

where P is the applied SPF force, r is the radius of the clamped area (2 mm), D is the flexural rigidity ($D = \frac{E \cdot t^3}{12(1-\nu^2)}$), t is the thickness (0.5 mm), E is the Young's modulus (110 GPa), ν is Poisson's ratio (0.31), e is the loaded area radius $e = \sqrt{R/y_{MAX}}$, and when $e < 0.5t$, $e' = (\sqrt{1.6e^2 + t^2})$. Fig. 11 plots the estimated σ_{MAX} at the disc surface against the SPF F_{MAX} based on Eqs. (1) and (2), with the relationship between σ_{MAX} and F_{MAX} over three times that determined by the correlation of the data sets above. Such large stresses would be expected due to the very small loading area associated with the initial stages of the SPF test. However, again these stresses exceed the σ_{UTS} of the material, so plastic deformation at the centre would be expected to occur almost instantaneously. Nonetheless, increases in specimen deflection and thus contact area reduce the stresses to magnitudes that appear more consistent with equivalent life UF tests, as presented in Fig. 11 for F_{MAX} = 500 N. Therefore, this clearly indicates that the stress throughout the entire specimen must be considered and analysed in a relatively stabilised condition in order to appropriately attempt to correlate SPF to UF results, specifically via Finite Element Analysis (FEA).

3.4.2. Numerical approaches

Whilst much literature has also been published on capturing the evolving stress state in a SP test using numerical approaches [30–32], there is currently no research available that is capable of modelling the stress evolution in a SP disc when subjected to a cyclic loading condition. FE analysis through DEFORM was used to simulate the cyclic response of Ti-6Al-4V under a SPF loading arrangement. The numerical model was developed using DEFORM standard code. To capture the specimen geometry of a miniature disc and the experimental set up as detailed earlier, an axisymmetric model was employed where the disc sample was clamped in a rigid die body along its entire contour. The outlay of the mesh adopted, and the components used are displayed in Fig. 12, where the specimen thickness was 500 µm, specimen diameter was 9.5 mm, punch diameters were 2 mm and the upper and lower receiving holes were 4 mm. Like the upper and lower die, the punch indenter was also modelled as a rigid body, insensitive to deformation in all degrees of freedom with horizontal or rotational movement also restricted. A model of 1000 CAX4 elements were used for the disc specimen, with a further refined mesh employed towards the contact area of the punch and specimen. The friction coefficient was set to a value of µ = 0.25, in line with the values used in existing literature [33,34] since this was found to produce more realistic results for deformation of a disc. Flow stress data for the specific Ti-6Al-4V variant tested was utilised to ensure an accurate representation of behaviour along with the implementation of a kinematic hardening approach.

Before performing the cyclic simulations, to determine whether the maximum stresses calculated from the above equations agreed, the specimen was modelled as an elastic body with load applied through the upper indenter for an R = 0.1 arrangement. Fig. 13 reveals the stress distribution, location and magnitude of the maximum stress for a load of 300 N and 1000 N and as expected, the maximum stress is located at the centre on the underside of the disc. The comparison of the DEFORM elastic model to the analytical equations is presented in Fig. 11 with the stresses in relatively good agreement, drifting further apart as the deflection increases as would be expected since the analytical equations were under the assumption of a small deflection compared to the disc thickness. As previously mentioned these stresses largely exceed the σ_{UTS} so careful consideration of the cyclic simulations along with the test piece deformation are paramount. Due to the complexity of the test setup and stress state, only the R = 0.1 cyclic simulations are presented. Fig. 14 shows the distribution of the mean strain and maximum principal stress across the Ti-6Al-4V specimen after 100 cycles (300 N and 1000 N), after which a relatively stabilised condition has been realised. The max principal stress at the location of the maximum mean strain is considered as it is from this point that failure would be expected to initiate.

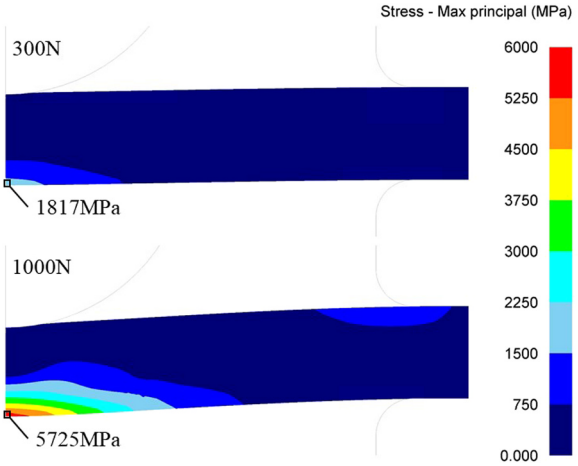

Fig. 13. Stress distribution, location and magnitude of the maximum principal stress when the specimen is considered an elastic for a 300 N and 1000 N load.

Fig. 13 shows that the σ_{UTS} is exceeded during the first cycle of the test, which is supported through previous research into small punch tensile testing of the same material [32], where fractography revealed plastic deformation and the onset of cracking on tests interrupted at displacements of 0.1 and 0.35 mm. This is further corroborated when

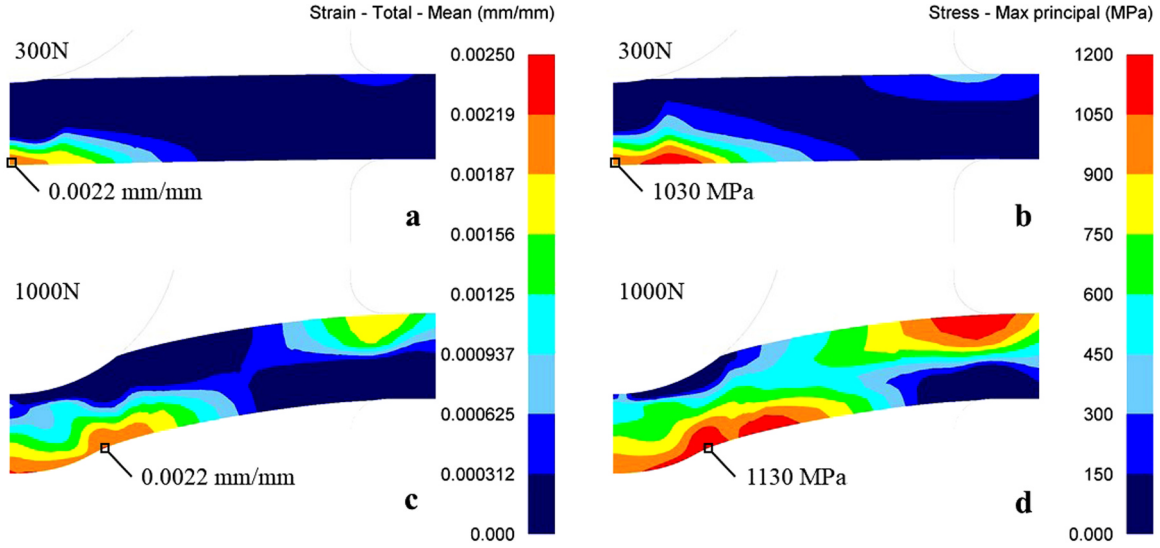

Fig. 14. Distribution of the mean strain and maximum principal stress across the specimen after 100 cycles for a) b) 300 N and c) d) 1000 N.

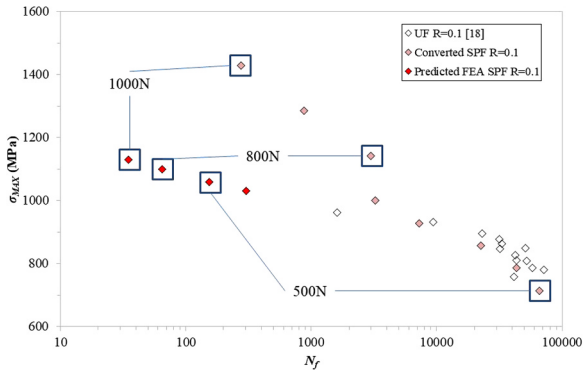

Fig. 15. Comparison of σ_{MAX} vs. N_f for UF, converted SPF based on an empirical approach ($\sigma_{MAX} = 1.54 \bullet F_{MAX}$) and predicted FEA SPF results based on a Goodman lifing approach.

implementing a Goodman mean stress lifing approach [35] which utilises the available UF data for the material and calculates the expected fatigue life for apparent stabilised maximum principal stress conditions, the results from which are presented in Fig. 15, along with indications of the SPF maximum load conditions. These very low fatigue lives determined by the Goodman approach from the FEA maximum principal stresses are to be expected with the material σ_{UTS} being 1046 MPa.

Nevertheless, the SPF experiments produce results and fractographic evidence that a fatigue type response is taking place throughout, as evidenced by the fractographic analysis. Therefore, the manner in which the apparent stabilised stress is determined by FEA requires further consideration since the challenges of the evolving biaxial stress state and the early onset of yielding and plastic deformation perhaps reveal the need for a damage criterion to be implemented into the FEA simulations. Additional benefit would come from having UF data in a range of fatigue lives similar to that produced by the SPF experiments.

4. Conclusions

In this paper, a highly bespoke SPF testing capability has been developed to determine the fatigue properties of the titanium alloy Ti-6Al-4V. A series of test results have been presented from novel experiments on the forged material variant from which representative hysteresis fatigue loops and time-displacement information was generated. The results showed good agreement with uniaxial fatigue data and fractographic investigations revealed features typical of traditional fatigue approaches. This included striations, which were observed in the R = 0.1 testing regime and a study found how striation counting produced a good interpretation of the crack growth rate and the proportion of fatigue life spent in initiation in such a geometry. FEA simulations, produced using DEFORM software, were carried out to determine the stresses in the initial stages of the test and then to capture the stress evolution seen in a SPF test. It is clear from the FEA simulations and previous research that plastic deformation and the onset of cracking is present during these initial stages and consequently the apparent stabilised stresses are close to or exceed the materials σ_{UTS}. This is an ongoing challenge since the evidence of striations reveal a fatigue like response is occurring. Overall, the proposed test methodology shows real promise for cyclic material property evaluation of geometries of limited dimension and is of real potential benefit to the mechanical characterisation community.

Acknowledgments

The current research was funded under the Engineering & Physical Sciences Research Council / Rolls-Royce Strategic Partnership in Structural Metallic Systems for Gas Turbines (grants EP/H500383/1 and EP/H022309/1). The provision of materials and supporting information from Rolls-Royce plc is gratefully acknowledged by the authors, together with the assistance provided by the Swansea University AIM Facility, which was funded in part by the EPSRC (grant EP/M028267/1). Mechanical tests were performed at Swansea Materials Research and Testing Ltd. (SMaRT). Requests for access to the underlying research data should be directed to the corresponding author and will be considered against commercial interests and data protection.

Author contributions

The work presented in this paper was carried out as a collaboration between all authors. The research theme was conceptualised by Robert Lancaster and Gavin Baxter. Robert Lancaster, Spencer Jeffs and Roger Hurst designed the small punch fatigue test configuration and Henry Illsley performed the mechanical testing, data curation and subsequent failure analysis. Spencer Jeffs, Christos Argyrakis and Henry Illsley derived the computational models. Robert Lancaster, Spencer Jeffs, Henry Illsley, Christos Argyrakis and Gavin Baxter co-worked on the writing of the original draft. Robert Lancaster and Spencer Jeffs reviewed and edited the revised manuscript. Robert Lancaster and Gavin

Baxter secured the appropriate funding and supervised the project administration. All authors have contributed to, seen and approved the final manuscript.

Conflicts of interest

The authors declare no conflict of interest.

References

[1] D. Blagoeva, Y.Z. Li, R.C. Hurst, Qualification of P91 welds through Small Punch creep testing, J. Nucl. Mater. 409 (2) (2011) 124–130.
[2] T. Bai, K. Guan, Evaluation of stress corrosion cracking susceptibility of nanocrystallized stainless steel 304L welded joint by small punch test, Mater. Des. 52 (2013) 849–860.
[3] C. Rodríguez, J. García Cabezas, E. Cárdenas, F.J. Belzunce, C. Betegón, Mechanical properties characterization of heat-affected zone using the small punch test, Weld. J. 88 (9) (2009) 188s–192s.
[4] W.R. Corwin, G.E. Lucas, The Use of small-scale specimens for testing irradiated material: a symposium sponsored by ASTM Committee E-10 on Nuclear Technology and Applications, Albuquerque, N.M., 23 Sept. 1983. ASTM, 1986.
[5] M.P. Manahan, A.S. Argon, O.K. Harling, The development of a miniaturizsed disk bend test for determination of post irradiation mechanical properties, J. Nucl. Mater. 104 (1981) 1545–1550.
[6] M.P. Manahan, A new post-irradiation mechanical behavior test - the miniaturized disk bend test, Nucl. Technol. 63 (2) (1983) 295–315.
[7] R.C. Hurst, R.J. Lancaster, S.P. Jeffs, M.R. Bache, The contribution of small punch testing towards the development of materials for aero-engine applications, Theor. Appl. Fract. Mech. 86 (2016) 69–77.
[8] P. Busquin, P. Argüelles, M. Bischoff, B. a.C. Droste, S. Evans, W. Kröll, J.-L. Lagardère, A. Lina, J. Lumsden, D. Ranque, S. Rasmussen, P. Reutlinger, S. Robins, H. Terho, A. Wittlöw, European aeronautics: a vision for 2020 — a synopsis, Air Sp. Eur. (2001) 16–18.
[9] L. Zhao, H. Jing, L. Xu, Y. Han, J. Xiu, Y. Qiao, Evaluating of creep property of distinct zones in P92 steel welded joint by small punch creep test, Mater. Des. 47 (2013) 677–686.
[10] D. Andrés, R. Lacalle, J.A. Álvarez, Creep property evaluation of light alloys by means of the Small Punch test: creep master curves, Mater. Des. 96 (2016) 122–130.
[11] CEN Workshop Agreement CWA 15267, European Code of Practise: Small Punch Test Method for Metallic Materials, 2007.
[12] M. Bruchhausen, S. Holmström, I. Simonovski, T. Austin, J.M. Lapetite, S. Ripplinger, F. de Haan, Recent developments in small punch testing: tensile properties and DBTT, Theor. Appl. Fract. Mech. 86 (2016) 2–10.
[13] S. Davies, S. Jeffs, R. Lancaster, G. Baxter, High temperature deformation mechanisms in a DLD nickel superalloy, Materials (Basel) 10 (5) (2017) 457.
[14] F. Dobeš, P. Dymáček, M. Besterci, Estimation of the mechanical properties of aluminium and an aluminium composite after equal channel angular pressing by means of the small punch test, Mater. Sci. Eng. A 626 (2015) 313–321.
[15] T.E. García, C. Rodríguez, F.J. Belzunce, C. Suárez, Estimation of the mechanical properties of metallic materials by means of the small punch test, J. Alloy. Compd. 582 (2014) 708–717.
[16] R.V. Prakash, Investigation of static and fatigue properties of materials through small specimen test methods, in: Proceedings of the 3rd International Conference on Small Scale Test Techniques, 2014, pp. 339–347.
[17] R.V. Prakash, Study of fatigue properties of materials through cyclic automated ball indentation and cyclic small punch test methods, Key Eng. Mater (2017) 273–284.
[18] M.T. Whittaker, W.J. Evans, R. Lancaster, W. Harrison, P.S. Webster, The effect of microstructure and texture on mechanical properties of Ti6-4, Int. J. Fatigue 31 (11–12) (2009) 2022–2030.
[19] G.Q. Wu, C.L. Shi, W. Sha, A.X. Sha, H.R. Jiang, Effect of microstructure on the fatigue properties of Ti-6Al-4V titanium alloys, Mater. Des. 46 (2013) 668–674.
[20] T.M. Mower, Degradation of titanium 6Al-4V fatigue strength due to electrical discharge machining, Int. J. Fatigue 64 (2014) 84–96.
[21] R. Lancaster, G. Davies, H. Illsley, S. Jeffs, G. Baxter, Structural integrity of an electron beam melted titanium alloy, Materials (Basel) 9 (6) (2016).
[22] S.D. Norris, J.D. Parker, Deformation processes during disc bend loading, Mater. Sci. Technol. 12 (1996) 163–170.
[23] E. Hershko, N. Mandelker, G. Gheorghiu, H. Sheinkopf, I. Cohen, O. Levy, Assessment of fatigue striation counting accuracy using high resolution scanning electron microscope, Eng. Fail. Anal. 15 (1–2) (2008) 20–27.
[24] M.F. Moreno, Application of small punch testing on the mechanical and microstructural characterizations of P91 steel at room temperature, Int. J. Press. Vessel. Pip. 142–143 (2016) 1–9.
[25] J.G. Kumar, K. Laha, Small punch creep deformation and rupture behavior of 316L (N) stainless steel, Mater. Sci. Eng. A 641 (2015) 315–322.
[26] J. Chakrabarty, A theory of stretch forming over hemispherical punch heads, Int. J. Mech. Sci. 12 (1970) 315–325.
[27] P. Dymáček, Recent developments in small punch testing: applications at elevated temperatures, Theor. Appl. Fract. Mech. 86 (2016) 25–33.
[28] S.P. Jeffs, R.J. Lancaster, Elevated temperature creep deformation of a single crystal superalloy through the small punch creep method, Mater. Sci. Eng. A 626 (2015) 330–337.
[29] E.J. Hearn, Mechanics of Materials 2: An Introduction to the Mechanics of Elastic and Plastic Deformation of Solids and Structural Materials, Third ed., Butterworth-Heinemann, Oxford, 1997.
[30] M. Abendroth, M. Kuna, Determination of ductile material properties by means of the small punch test and neural networks, Adv. Eng. Mater. 6 (7) (2004) 536–540.
[31] P. Dymáček, K. Milička, Creep small-punch testing and its numerical simulations, Mater. Sci. Eng. A 510–511 (. 2009) 444–449.
[32] R.J. Lancaster, H.W. Illsley, G.R. Davies, S.P. Jeffs, G.J. Baxter, Modelling the small punch tensile behaviour of an aerospace alloy, Mater. Sci. Technol. 33 (9) (2017) 1065–1073.
[33] C. Soyarslan, B. Gülçimen, S. Bargmann, P. Hähner, Modeling of fracture in small punch tests for small- and large-scale yielding conditions at various temperatures, Int. J. Mech. Sci. 106 (2016) 266–285.
[34] Y. Xu, T. Xu, K. Guan, Y. Lu, Prediction of cleavage fracture in ferritic steels by small punch tests with a modified Weibull stress model, Eng. Fract. Mech. 124–125 (2014) 97–111.
[35] S. Suresh, Fatigue of Materials, Second ed., Cambridge University Press, 1998.